



Controlled Synthesis of Two-Dimensional 1T-TiSe₂ with Charge Density Wave Transition by Chemical Vapor Transport

Jingyi Wang,^{†,§} Husong Zheng,^{‡,§} Guanchen Xu,[†] Lifei Sun,[†] Dake Hu,[†] Zhixing Lu,[†] Lina Liu,[†] Jingying Zheng,[†] Chenggang Tao,^{*,‡} and Liying Jiao^{*,†} 

[†]Key Laboratory of Organic Optoelectronics and Molecular Engineering of the Ministry of Education, Department of Chemistry, Tsinghua University, Beijing 100084, China

[‡]Department of Physics, Center for Soft Matter and Biological Physics, Virginia Polytechnic Institute and State University, Blacksburg, Virginia 24061, United States

 Supporting Information

ABSTRACT: Two-dimensional (2D) metallic transition metal dichalcogenides (TMDCs), such as 1T-TiSe₂, are ideal systems for exploring the fundamentals in condensed matter physics. However, controlled synthesis of these ultrathin materials has not been achieved. Here, we explored the synthesis of charge density wave (CDW)-bearing 2D TiSe₂ with chemical vapor transport (CVT) by extending this bulk crystal growth approach to the surface growth of TiSe₂ by introducing suitable growth substrates and dramatically slowing down the growth rate. Sub-10 nm TiSe₂ flakes were successfully obtained, showing comparable quality to the mechanically exfoliated thin flakes. A CDW state with 2 × 2 superstructure was clearly observed on these ultrathin flakes by scanning tunneling microscopy (STM), and the phase transition temperature of these flakes was investigated by transport measurements, confirming the existence of CDW states. Our work opens up a new approach to synthesizing 2D CDW and superconductive TMDCs for exploring new fundamentals and applications in novel electronics.

Two-dimensional (2D) semiconducting transition metal dichalcogenides (TMDCs), such as MoS₂ and WS₂, have attracted considerable interest due to their potential applications in next-generation electronics,¹ optoelectronics,² photovoltaic devices,³ and so on. Beyond semiconducting TMDCs, 2D metallic TMDCs such as 1T-TiSe₂,^{4–7} 2H-NbSe₂,^{8–10} 1T-TaS₂,^{11,12} and 1T-TaSe₂^{13–15} have recently emerged as unique platforms for exploring their exciting properties of superconductivity and charge density wave (CDW) at low dimension. These ultrathin metallic TMDCs films behaved dramatically differently from their bulk counterparts due to their unique 2D plenary structures and thus provided important insights into the origins of superconductivity and CDW in TMDCs which have been a longstanding question in condensed matter physics.^{16–18} Among these metallic TMDCs, TiSe₂ is a typical CDW material which undergoes a CDW phase transition at ~200 K accompanied by the formation of a 2 × 2 × 2 superstructure, and the CDW order can be suppressed and replaced with superconducting (SC) order via external modulations, such as doping and pressure.^{16,17} Very recently, the phase transitions of ultrathin 2D TiSe₂ have been explored with both angle-resolved

photoemission spectroscopy (ARPES)^{5,6} and electrical measurements,⁷ revealing distinct CDW phase transitions in these 2D atomic layers. More importantly, the 2D nature of ultrathin TiSe₂ flakes allows for the modulation of many body states by external electric field, and consequently, the details of the CDW/SC phase transitions of TiSe₂ can be tuned by electric-field effect,⁷ which is a remarkable leap toward the applications of 2D TMDCs in CDW collective states and superconductivity devices. The key challenge for the practical applications of these 2D TMDCs remains controllable synthesis, as the chemical synthesis of pristine 2D CDW/SC TMDCs has not been achieved to date. Chemical vapor deposition (CVD) has been successfully employed to grow ultrathin semiconducting TMDCs such as MoS₂ and WSe₂,^{19,20} but it is not feasible to synthesize high quality metallic TMDCs by conventional CVD approach due to the very high tendency of oxidation for these materials.^{7,9,11} Molecular beam epitaxy (MBE) has been utilized to deposit TiSe₂ thin films on graphene;^{4–6} however, this approach is not capable of growing pristine TiSe₂ on insulating substrates without graphene which may significantly affect the phase transitions.^{5,6} Therefore, it is highly desired to develop controllable chemical methods to synthesize pristine ultrathin TiSe₂ flakes for making this emerging material easily accessible for exploring new fundamentals in both condensed matter physics and device physics.

Here, we explored the surface growth of ultrathin highly crystalline CDW/SC TMDCs with 1T-TiSe₂ as an example with chemical vapor transport (CVT) by carefully controlling the mass transport during the growth. For the first time, sub-10 nm pristine 2D TiSe₂ flakes were obtained by chemical synthesis and these flakes showed very high quality as indicated by scanning tunneling microscopy (STM) characterizations. Moreover, the characteristic feature of the 2 × 2 superstructure for the CDW phase of TiSe₂ was clearly observed by STM on our samples at 77 K, indicating that well-ordered CDW states occurred at low temperature in the chemically synthesized ultrathin TiSe₂ flakes. Our work paves the way for the controllable synthesis of 2D CDW/SC TMDCs and thus will greatly extend the functionalities and applications of 2D atomic crystals.

Received: October 5, 2016

Published: November 29, 2016

CVT is the most reliable approach for growing high quality TMDCs single crystals for both research and commercial purposes.²¹ Although this approach has been intensively studied for decades for growing bulk crystals, it has never been demonstrated on synthesizing 2D TMDCs. A typical CVT growth of single crystals of TMDCs involves the volatilization and reactions of solid precursors with the aid of transport agent and the deposition of the products in the form of single crystals driven by a temperature gradient between the source and the growth zone in a sealed quartz ampule.²¹ In order to acquire the ultrathin flakes instead of bulk crystals using the CVT method, it is essential to introduce a growth substrate to guide the 2D growth of TMDCs and dramatically slow down the growth rate. According to intensive studies on the kinetics of single crystals growth by CVT, the growth rate of single crystals is controlled by the mass transport of reactants via gas motion from the source zone to the growth zone through diffusion or convection.²¹ In our experiments, the ampule lies horizontally and the pressure inside the ampule is $<2 \times 10^4$ Pa, so the mass transport is dominated by diffusion instead of convection and, therefore, the transport rate J can be described with Schaefer's transport equation.²²

$$J \propto \frac{p_i}{\sum p_i} \cdot \frac{s}{l} \cdot \bar{T}^{0.75}$$

p_i is the partial pressure of the transport effective species, which is dependent on the amounts of transport agent and chalcogenide; s and l are the cross-section and length of the diffusion path, respectively; and \bar{T} is the average temperature of T_1 and T_2 . Therefore, compared with conventional CVT growth, we should minimize the amounts of transport agent, increase the length of diffusion while decrease the cross-section of the diffusion path and reduce the average temperature to slow down the mass transport and enable the growth of 2D TiSe₂. Besides these, choosing suitable transport agent with lower transport capability is the most efficient way to slow down the growth rate of TiSe₂. I₂ is the most-widely used transport agent for conventional CVT growth, but it is not feasible to grow ultrathin TiSe₂ with I₂ due to its too high transport ability (Figure S2). After a few tries, we found AgCl was the most suitable transport agent as it decomposes to produce Cl₂ at a suitable temperature which allows for slow mass transport (see more discussions in Supporting Information).

Based on the above discussions, we designed the setup for the surface growth of TiSe₂ thin flakes with the CVT method as schematically illustrated in Figure 1a. To start with the synthesis, ultrapure Ti, Se, and AgCl powders (~5.0 mg in total) were mixed at an appropriate ratio and then sealed in an evacuated quartz ampule at a pressure of $<1.5 \times 10^{-4}$ Pa together with a sapphire substrate at the other end, separated by a neck on the ampule. After the sealing, the ampule was loaded into a two-zone furnace and the distance between the growth precursor and substrate was well-adjusted to ensure that the temperatures for the source and growth regions were 800 and 780 °C, respectively. By optimizing the growth parameters including substrate (Figure S2), the amount of AgCl (Figure S3), growth temperature (Figure S4), and heating up and cooling down rates (Figure S5), very slow growth of TiSe₂ has been achieved, which allows for the controllable synthesis of ultrathin TiSe₂ flakes by tuning the growth duration. After growing for 5 min at the optimized conditions, ultrathin TiSe₂ flakes in half-hexagonal shape with a thickness of ~3.0–8.0 nm and length of ~4.0–10.0 μm were

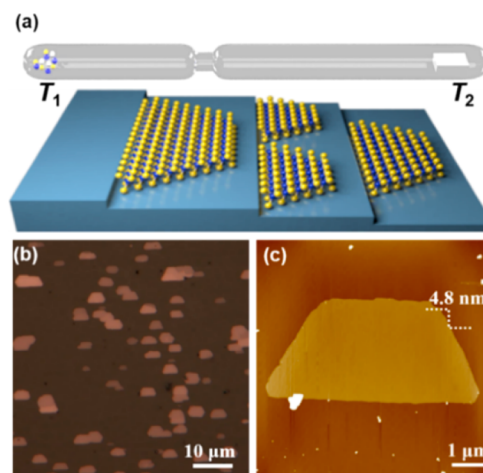


Figure 1. Synthesis of ultrathin TiSe₂ flakes using CVT method. (a) Schematic for the setup of surface growth of 2D TiSe₂ with CVT method and the obtained TiSe₂ thin flakes, showing the nucleation and growth of TiSe₂ are guided by the step edges on sapphire. (b and c) Optical and AFM images of the as-grown TiSe₂ flakes on the C-plane sapphire substrate which show half-hexagonal shapes with preferred orientations on the substrate.

observed at a high density by both optical microscopy and atomic force microscopy (AFM) (Figure 1b–c, Figure S8). Obviously, these TiSe₂ flakes oriented along the same direction which is parallel to the step edges of the C-plane sapphire substrate (Figure S6), suggesting an epitaxial growth process. In contrast to the growth on sapphire, ultrathin TiSe₂ flakes grown on the mica substrate under the same growth conditions showed triangular shape (Figure S7). Therefore, we concluded that growth of ultrathin TiSe₂ flakes on sapphire substrates was guided by the step edges on the substrates in a similar way to the previously reported growth of WSe₂ on sapphire.²³

Micro-Raman spectroscopy is utilized to identify and characterize the obtained TiSe₂ flakes. The as-grown TiSe₂ flakes showed two Raman peaks at ~134 cm⁻¹ and ~198 cm⁻¹ which were assigned to E_g and A_{1g} mode,²⁴ respectively, under 632.8 nm excitation (Figure 2a), consistent with the Raman peaks of the bulk TiSe₂ crystals.²⁴ Different from MoS₂ and many other 2D TMDCs,²⁵ the Raman peak positions of TiSe₂ ultrathin flakes for both E_g and A_{1g} modes did not show obvious dependence on the thickness down to 4.5 nm (Figure 2a). To evaluate the uniformity of the TiSe₂ ultrathin flakes, we generated a Raman mapping image with ~198 cm⁻¹ (strongest peak of TiSe₂) on the TiSe₂ flakes (Figure 2b), and the obtained mapping image showed uniform Raman intensity across the whole flake, confirming the high uniformity of our as-grown TiSe₂ flakes. X-ray diffraction (XRD) was used to study the crystal structure of as-made TiSe₂ flakes. The peaks of our as-grown 2D TiSe₂ were consistent with the TiSe₂ crystal grown by the CVT method using I₂ as the transport agent, confirming the formation of single crystalline TiSe₂ thin flakes by our approach (Figure S9). To rule out the possible residue of Ag or Cl elements in our TiSe₂ flakes, we measured individual TiSe₂ flakes (>10 flakes) with nano-Auger electron spectroscopy (AES). The obtained results confirmed that no Ag or Cl element was detected by AES and the measured Se:Ti ratio was ~2.03, very close to the stoichiometric ratio of 2.0 for TiSe₂, further confirming the high purity of our samples.

We then characterized the atomic crystal structure of the as-grown TiSe₂ flakes (~5.0 nm thick) with STM at both room

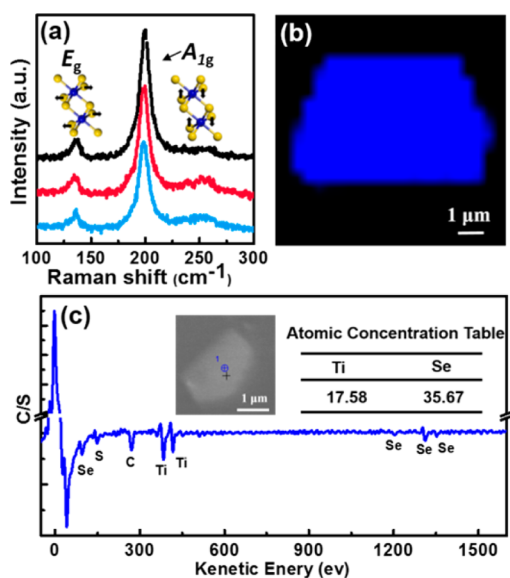


Figure 2. Raman and Auger electron spectroscopy characterizations of the CVT-grown ultrathin TiSe₂ flakes. (a) Typical Raman spectra of the TiSe₂ flakes with varied thickness of 4.5 nm, 6.5 and 12.0 nm, from bottom to top. Insets, the unit cell of the TiSe₂ lattice and the main phonon mode vectors. (b) Raman mapping image of a ~4.2-nm-thick flake with 198 cm⁻¹ peak intensity. (c) Auger electron spectrum of an as-grown 2D TiSe₂ flake as shown in the inset. To avoid charging effect during the measurements, a thin layer conductive polymer of Elektra 92 (SX AR-PC 5000/90.2) was spin-coated on the samples, and the detected S and C elements were originated from the polymer.

temperature and low temperature. To obtain the intrinsic surface structure of the TiSe₂ flakes, we deposited metal contacts to the flakes grown on sapphire using a shadow mask for direct STM imaging without transferring them to conducting substrates (Figure S1). The large-scale STM image in Figure 3b of the as-grown TiSe₂ flakes obtained at room temperature shows a very smooth surface compared with the films grown by MBE,^{4,6} and in some regions small vacancy islands were resolved with a depth of ~0.6 nm, in accordance with the *c*-axis unit-cell length of bulk

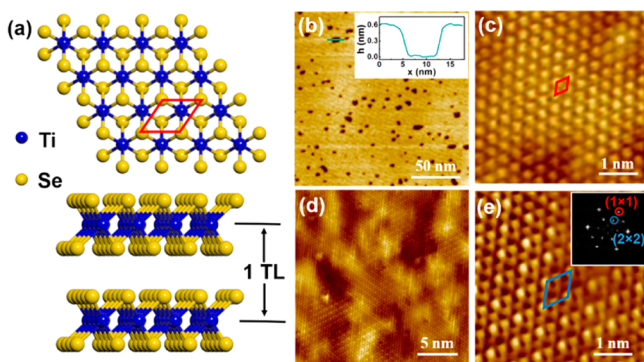


Figure 3. STM imaging of CVT-grown ultrathin TiSe₂ flakes. (a) Schematic crystal structure of 1T-TiSe₂. (b) Large-scale STM topographic image of the as-grown TiSe₂ flakes at room temperature ($V_s = 1.0$ V, $I = 0.2$ nA). The inset is the line profile crossing a vacancy island marked by the green line. (c) Atomically resolved STM topographic image at room temperature ($V_s = 0.4$ V, $I = 1.0$ nA). (d and e) At $T = 77$ K, atomically resolved STM topographic images ((d) $V_s = 0.2$ V, $I = 0.3$ nA and (e) $V_s = 0.1$ V, $I = 0.4$ nA). Inset, the corresponding FFT image of (e). The corresponding filled state STM image is shown in Figure S10b.

TiSe₂ as sketched in Figure 3a, which may be originated from the defects formed during the growth or by postgrowth surface oxidation; the estimated defect density is $(7.7 \pm 3.9) \times 10^{-2}$ nm⁻² (Figure S10a). The atomically resolved STM image shows well-ordered hexagonal packing of Se atoms with an interatomic spacing of 3.5 ± 0.1 Å (Figure 3c), consistent with the atomic structure of 1T-TiSe₂ as illustrated in Figure 3a. At $T = 77$ K, the atomically resolved STM images and corresponding 2D fast Fourier transform (FFT) image reveal a 2×2 superlattice, suggesting the occurrence of CDW order at low temperature (Figure 3d and 3e).^{26,27} The existence of the well-ordered CDW phase at 77 K in our synthesized ultrathin TiSe₂ flakes strongly supports the high quality of our sample.

To accurately determine the CDW phase transition temperature (T_{CDW}) of the ultrathin TiSe₂ flakes, we fabricated multiple-terminal devices on these flakes with electron beam lithography (EBL) and metal deposition and carried out electrical measurements at varied temperature from 77 to 300 K. The four-terminal resistance–temperature (R – T) plot of a typical TiSe₂ flake with a thickness of ~8.0 nm (Figure 4a and Figure 4b) showed a

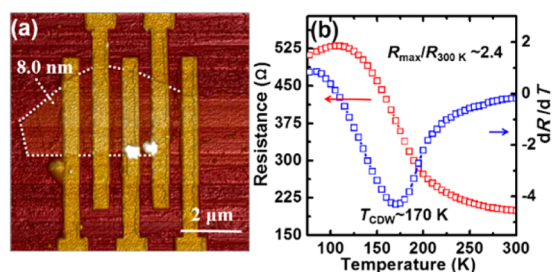


Figure 4. CDW phase transition temperature measurements on the CVT-grown ultrathin TiSe₂ flakes. (a) AFM image of a typical multiple-terminal device of an as-grown TiSe₂ flake with a thickness of ~8.0 nm (b) Temperature dependence of the resistance of the TiSe₂ device shown in (a). Blue curve (dR/dT) denotes the derivative of the resistance with the temperature, and the minimum value of the (dR/dT) indicates the T_{CDW} of this flake is ~170 K.²⁸

similar line shape to both bulk crystals and mechanically exfoliated flakes.^{7,16,17} The R – T curve presented a broad maximum at ~105 K with the ratio R_{max}/R_{300K} of 2.4. This ratio has been widely used to evaluate the quality of TiSe₂ single crystals;¹⁶ the ratio for our TiSe₂ thin flakes is higher than the mechanically exfoliated ones (<1.5),⁷ again indicating the high quality of our CVT-made TiSe₂ flakes. We noticed that our CVT-grown TiSe₂ ultrathin flakes exhibited a CDW phase transition at ~170 K which is the same as the T_{CDW} of exfoliated flakes⁷ with similar thickness, but dramatically lower than that of the bulk crystals of ~200 K, which may be attributed to the reduced thickness. Recently, two independent studies on the CDW transition in 2D stacks of TiSe₂/graphene measured by ARPES reported dramatically different CDW transition temperatures of ~232 K⁵ and ~200 K,⁶ respectively. The inconsistencies of the measured transition temperatures of ultrathin TiSe₂ reported by different groups may be attributed to the varied substrates, defect densities, doping concentrations, and measuring methods, and further studies on the origins of these differences may provide new insights into the manipulation of phase diagrams of these 2D CDW/superconducting materials.

In summary, we developed a new approach for the controllable synthesis of high quality 2D TMDCs by adapting the CVT approach to the surface growth of 2D atomic layers through

optimizing transport agents, growth substrates, growth temperature, and other growth parameters in chemical vapor transport reactions. With this approach, the controllable synthesis of pristine ultrathin TiSe₂ flakes has been realized. The as-grown ultrathin TiSe₂ flakes exhibited very high crystallinity, comparable to mechanically exfoliated thin TiSe₂ flakes, as characterized by various approaches. The occurrence of CDW order accompanied by surface reconstruction was clearly visualized by the atomically resolved STM imaging at ~77 K, and the CDW phase transition temperature of the CVT-grown TiSe₂ was also accurately measured with variable-temperature transport measurements. This first observation of the CDW phase in chemically synthesized pristine TiSe₂ ultrathin flakes presents a significant step toward the practical applications of the 2D CDW/superconducting materials. Moreover, in principle, all TMDCs that can be grown in the form of single crystals by CVT can also be grown into 2D form by adjusting the growth parameters as we demonstrated in this work. Therefore, we believe that, in parallel with CVD synthesis, CVT will become another universal method for growing various 2D atomic crystals to further extend the family of 2D materials.

■ ASSOCIATED CONTENT

📄 Supporting Information

The Supporting Information is available free of charge on the ACS Publications website at DOI: 10.1021/jacs.6b10414.

Experimental details, supporting figures and discussions
(PDF)

■ AUTHOR INFORMATION

Corresponding Authors

*cgtao@vt.edu

*lyjiao@mail.tsinghua.edu.cn

ORCID

Liyang Jiao: 0000-0002-6576-906X

Author Contributions

[§]J.W. and H.Z. contributed equally.

Notes

The authors declare no competing financial interest.

■ ACKNOWLEDGMENTS

L.J. acknowledges National Natural Science Foundation of China (Nos. 21322303, 51372134, 21573125) and Tsinghua University Initiative Scientific Research Program. H.Z. and C.T. acknowledge the financial support provided for this work by the U.S. Army Research Office under the grant W911NF-15-1-0414.

■ REFERENCES

- (1) Geim, A. K.; Grigorieva, I. V. *Nature* **2013**, *499*, 419.
- (2) Britnell, L.; Ribeiro, R. M.; Eckmann, A.; Jalil, R.; Belle, B. D.; Mishchenko, A.; Kim, Y.; Gorbachev, R. V.; Georgiou, T.; Morozov, S. V.; Grigorenko, A. N.; Geim, A. K.; Casiraghi, C.; Neto, A. H. C.; Novoselov, K. S. *Science* **2013**, *340*, 1311.
- (3) Wu, Y. B.; Yang, W.; Wang, T. B.; Deng, X. H.; Liu, J. T. *Sci. Rep.* **2016**, *6*, 20955.
- (4) Peng, J. P.; Guan, J. Q.; Zhang, H. M.; Song, C. L.; Wang, L. L.; He, K.; Xue, Q. K.; Ma, X. C. *Phys. Rev. B: Condens. Matter Mater. Phys.* **2015**, *91*, 121113.
- (5) Chen, P.; Chan, Y. H.; Fang, X. Y.; Zhang, Y.; Chou, M. Y.; Mo, S. K.; Hussain, Z.; Fedorov, A. V.; Chiang, T. C. *Nat. Commun.* **2015**, *6*, 8943.

- (6) Sugawara, K.; Nakata, Y.; Shimizu, R.; Han, P.; Hitosugi, T.; Sato, T.; Takahashi, T. *ACS Nano* **2016**, *10*, 1341.
- (7) Li, L. J.; O'Farrell, E. C. T.; Loh, K. P.; Eda, G.; Özyilmaz, B.; Neto, A. H. C. *Nature* **2015**, *529*, 185.
- (8) Xi, X.; Zhao, L.; Wang, Z.; Berger, H.; Forró, L.; Shan, J.; Mak, K. F. *Nat. Nanotechnol.* **2015**, *10*, 765.
- (9) Xi, X.; Wang, Z.; Zhao, W.; Park, J. H.; Law, K. T.; Berger, H.; Forró, L.; Shan, J.; Mak, K. F. *Nat. Phys.* **2015**, *12*, 139.
- (10) Ugeda, M. M.; Bradley, A. J.; Zhang, Y.; Onishi, S.; Chen, Y.; Ruan, W.; Ojeda-aristizabal, C.; Ryu, H.; Edmonds, M. T.; Tsai, H.; Riss, A.; Mo, S.; Lee, D.; Zettl, A.; Hussain, Z.; Shen, Z.; Crommie, M. F. *Nat. Phys.* **2015**, *12*, 92.
- (11) Yu, Y.; Yang, F.; Lu, X. F.; Yan, Y. J.; Cho, Y.; Ma, L.; Niu, X.; Kim, S.; Son, Y.; Feng, D.; Li, S.; Cheong, S.; Chen, X. H.; Zhang, Y. *Nat. Nanotechnol.* **2015**, *10*, 270.
- (12) Liu, G.; Debnath, B.; Pope, T. R.; Salguero, T. T.; Lake, R. K.; Balandin, A. A. *Nat. Nanotechnol.* **2016**, *11*, 845.
- (13) Yan, Z.; Jiang, C.; Pope, T. R.; Tsang, C. F.; Stickney, J. L.; Goli, P.; Renteria, J.; Salguero, T. T.; Balandin, A. A. *J. Appl. Phys.* **2013**, *114*, 204301.
- (14) Renteria, J.; Samnakay, R.; Jiang, C.; Pope, T. R.; Goli, P.; Yan, Z.; Wickramaratne, D.; Salguero, T. T.; Khitun, A. G.; Lake, R. K.; Balandin, A. A. *J. Appl. Phys.* **2014**, *115*, 034305.
- (15) Samnakay, R.; Wickramaratne, D.; Pope, T. R.; Lake, R. K.; Salguero, T. T.; Balandin, A. A. *Nano Lett.* **2015**, *15*, 2965.
- (16) Morosan, E.; Zandbergen, H. W.; Dennis, B. S.; Bos, J. W. G.; Onose, Y.; Klimczuk, T.; Ramirez, A. P.; Ong, N. P.; Cava, R. J. *Nat. Phys.* **2006**, *2*, 544.
- (17) Kusmartseva, A. F.; Sipos, B.; Berger, H.; Forro, L.; Tutis, E. *Phys. Rev. Lett.* **2009**, *103*, 23401.
- (18) Chang, J.; Blackburn, E.; Holmes, A. T.; Christensen, N. B.; Larsen, J.; Mesot, J.; Liang, R. X.; Bonn, D. A.; Hardy, W. N.; Watenphul, A.; Zimmermann, M. V.; Forgan, E. M.; Hayden, S. M. *Nat. Phys.* **2012**, *8*, 871.
- (19) Wang, X. S.; Feng, H. B.; Wu, Y. M.; Jiao, L. Y. *J. Am. Chem. Soc.* **2013**, *135*, 5304.
- (20) Li, M. Y.; Shi, Y.; Cheng, C. C.; Lu, L. S.; Lin, Y. C.; Tang, H. L.; Tsai, M. L.; Chu, C. W.; Wei, K. H.; He, J. H.; Chang, W. H.; Suenaga, K.; Li, L. J. *Science* **2015**, *349*, 524.
- (21) Lévy, F. *Crystallography and crystal chemistry of materials with layered structure*; D. Reidel Publishing Company: Dordrecht, The Netherlands, 1976.
- (22) Köpfe, R.; Steiner, J.; Schnöckel, H. Z. *Z. Anorg. Allg. Chem.* **2003**, *629*, 2168.
- (23) Chen, L.; Liu, B.; Ge, M.; Ma, Y.; Abbas, A. N.; Zhou, C. *ACS Nano* **2015**, *9*, 8368.
- (24) Sugai, S.; Murase, R.; Uchida, S.; Tanaka, S. *Solid State Commun.* **1980**, *35*, 433.
- (25) Zhang, X.; Qiao, X. F.; Shi, W.; Wu, J. B.; Jiang, D. S.; Tan, P. H. *Chem. Soc. Rev.* **2015**, *44*, 2757.
- (26) Hildebrand, B.; Didiot, C.; Novello, A. M.; Monney, G.; Scarfato, A.; Ubaldini, A.; Berger, H.; Bowler, D. R.; Renner, C.; Aebi, P. *Phys. Rev. Lett.* **2014**, *112*, 197001.
- (27) Novello, A. M.; Hildebrand, B.; Scarfato, A.; Didiot, C.; Monney, G.; Ubaldini, A.; Berger, H.; Bowler, D. R.; Aebi, P.; Renner, C. *Phys. Rev. B: Condens. Matter Mater. Phys.* **2015**, *92*, 081101.
- (28) Di Salvo, F. J.; Moncton, D. E.; Waszczak, J. V. *Phys. Rev. B* **1976**, *14*, 4321.